Acta Crystallographica Section C
Crystal Structure Communications
ISSN 0108-2701

Synthetic aenigmatite analog $Na_2(Mn_{5.26}Na_{0.74})Ge_6O_{20}$: structure and crystal chemical considerations

Günther J. Redhammer,[a]* Georg Roth,[b] Dan Topa[a] and Georg Amthauer[a]

[a]Department of Materials Engineering and Physics, Division of Mineralogy, University of Salzburg, Hellbrunnerstrasse 34, A-5020 Salzburg, Austria, and [b]Institute of Crystallography, RWTH Aachen University, Jägerstrasse 17/19, D-52056 Aachen, Germany
Correspondence e-mail: guenther.redhammer@aon.at

Received 29 September 2007
Accepted 21 December 2007
Online 9 February 2008

Disodium hexamanganese(II,III) germanate is the first aenigmatite-type compound with significant amounts of manganese. $Na_2(Mn_{5.26}Na_{0.74})Ge_6O_{20}$ is triclinic and contains two different Na positions, six Ge positions and 20 O positions (all with site symmetry 1 on general position 2*i* of space group $P\overline{1}$). Five out of the seven *M* positions are also on general position 2*i*, while the remaining two have site symmetry $\overline{1}$ (Wyckoff positions 1*f* and 1*c*). The structure can be described in terms of two different layers, *A* and *B*, stacked along the [011] direction. Layer *A* contains pyroxene-like chains and isolated octahedra, while layer *B* is built up by slabs of edge-sharing octahedra connected to one another by bands of Na polyhedra. The GeO_4 tetrahedra show slight polyhedral distortion and are among the most regular found so far in germanate compounds. The *M* sites of layer *A* are occupied by highly charged (trivalent) cations, while in layer *B* a central pyroxene-like zigzag chain can be identified, which contains divalent (or low-charged) cations. This applies to the aenigmatite-type compounds in general and to the title compound in particular.

Comment

Syntheses and crystal chemical investigations in the system of 1:3 Na and Li transition-metal germanate pyroxenes have shown that at ambient pressures pyroxene phases $NaM^{3+}Ge_2O_6$ (*M* = Cr, Fe, Sc and In) and $LiM^{3+}Ge_2O_6$ (*M* = Al, Ga, Cr, Fe, Sc and In) can be grown as high-quality single crystals using high-temperature solution (flux) techniques (Redhammer *et al.*, 2008). To extend the range of *M*-cationic substitution in clinopyroxene, the crystallization of Mn^{3+}-bearing Na germanate pyroxenes was attempted, but it was found that the pyroxene structure is not stable; instead, crystals of a new aenigmatite-type phase have been formed, whose crystal structure is described here.

The triclinic aenigmatite group of compounds can be summarized with the general formula $A_2B_6T_6O_{20}$, where *A* = Na or Ca in six-to-eightfold coordination, *B* is octahedrally coordinated Fe^{2+}, Fe^{3+}, Mg, Al, Cr, Ti^{4+} or Sb^{5+}, and *T* is tetrahedrally coordinated Si, Al, B or Be. The mineral group comprises several naturally occurring minerals, such as aenigmatite itself, $Na_2Fe_5TiSi_6O_{20}$ (Cannillo *et al.*, 1971), wilkinsonite, $Na_2Fe_4^{2+}Fe_2^{3+}Si_6O_{20}$ (Burt *et al.*, 2007), krinovite, $Na_2Mg_4Cr_2Si_6O_{20}$ (Merlino, 1972; Bonaccorsi *et al.*, 1989), rhönite, $Ca_2(Mg,Fe,Ti)_6Si_6O_{20}$ (Bonaccorsi *et al.*, 1990), or sapphirine-1Tc, $(MgAl)_8Si_6O_{20}$ (Merlino, 1980); a detailed review of the aenigmatite group is given by Kunzmann (1999). Additionally, the crystal structures of several Be-containing minerals, closely related to the aenigmatite group, have been refined recently, among them surinamite, $(Mg,Fe^{2+})_3Al_4BeSi_3O_{16}$ (Barbier *et al.*, 2002), makarochinite, $Ca_2Fe_4^{2+}Fe^{3+}TiSi_6O_{20}$ (Grew *et al.*, 2005), and welshite, $Ca_2Mg_4Fe^{3+}Sb^{5+}Si_4Be_2O_{20}$ (Grew *et al.*, 2007). Besides the naturally occurring species, Barbier (1995) reported the synthetic aenigmatite analog germanate, $Na_2(Mg,Fe)_6(Ge,Fe)_6O_{18}O_2$, while Yang & Konzett (2000) describe $Na_2Mg_6Si_6O_{18}(OH)_2$ and Gasparik *et al.* (1999) report $Na_2(Mg_{4.31}Si_{0.39}Fe_{1.3})Si_6O_{20}$. The title compound is of special interest as it is the first aenigmatite-type material containing Mn as the dominant octahedral cation.

The structure of $Na_2(Mn_{5.26}Na_{0.74})Ge_6O_{20}$ contains six distinct octahedrally coordinated *M* (*M* = Mn and Na) sites,

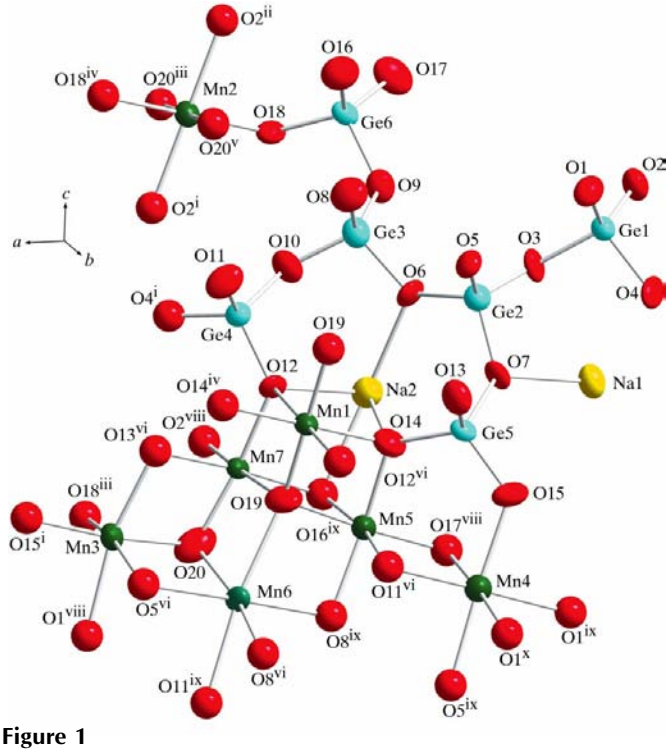

Figure 1
A view of the asymmetric unit and some symmetry-related atoms of the title compound, showing 95% probability displacement ellipsoids and the atomic numbering scheme. [Symmetry codes: (i) $x+1, y, z$; (ii) $-x, -y+1, -z+2$; (iii) $-x+1, -y+1, -z+1$; (iv) $-x+1, -y+1, -z+2$; (v) $x, y, z+1$; (vi) $-x+1, -y+2, -z+1$; (viii) $x+1, y, z-1$; (ix) $x, y, z-1$; (x) $-x, -y+2, -z+1$.]

 DOI: 10.1107/S0108270107068011

two different sevenfold-coordinated Na sites, six distinct Ge sites and 20 O-atom positions. An anisotropic displacement plot, containing the atomic nomenclature, is given in Fig. 1. The structural topology is described in terms of two layers stacked alternately along the [011] direction (Fig. 2). The first layer, labelled layer *A* from here on, contains pyroxene-like chains (Ge1–Ge4) extending in the [100] direction with two additional corner-sharing GeO_4 tetrahedra attached laterally (Fig. 3*a*). Within this layer, the tetrahedral chains are connected by isolated octahedra (Mn1 and Mn2). The second layer (layer *B*) is formed by infinite slabs of edge-sharing octahedra extending along *a* (*M*3–*M*7). These slabs are linked by 'bands' of Na polyhedra (Fig. 3*b*).

The average Ge—O bond lengths within the tetrahedral chain of layer *A* are similar (~1.741–1.747 Å), except for the Ge3 site, where the average is somewhat smaller (Table 1). This is due to a very small Ge3—O8 bond length [1.699 (5) Å]. Atom O8 is common to the Ge3, the *M*5 and two *M*6 polyhedra. The *M*6 sites, hosting Na^+ cations, exhibit a low valence sum (Brese & O'Keeffe, 1991) of 1.47 valence units (v.u.) and are only weakly bound to atom O8; they contribute 0.34 and 0.22 v.u to the valence sum of atom O8. Thus, the remaining two bonds of O8 to Ge3 and *M*5 are expected to be stronger and thus shorter. The Ge1 and Ge4 tetrahedra have two Ge—O bridging (br) bonds, the Ge—O_{br} distance being typically longer than the nonbridging (nbr) Ge—O_{nbr} distances. This is most evident for the Ge1 tetrahedron, with two short [⟨Ge—O_{nbr}⟩ = 1.723 (5) Å] and two long [⟨Ge—O_{br}⟩ = 1.772 (5) Å] bonds. The Ge2 and Ge3 tetrahedra have three bridging bonds with neighboring tetrahedra, with ⟨Ge—O_{br}⟩ distances of 1.753 (5) and 1.744 (5) Å, respectively; the difference Δ_{br} = ⟨Ge—O_{br}⟩ − ⟨Ge—O_{nbr}⟩ is 0.047 and 0.045 Å for Ge2 and Ge3, respectively.

Synthetic $Na_2(Mg_{3.6}Fe_{2.4})[(Ge_{5.6}Fe_{0.4})O_{18}]O_2$ shows a more uniform distribution of individual Ge—O bond lengths, ranging between 1.722 (2) and 1.781 (2) Å (Barbier, 1995). The $\langle Ge—O\rangle_{br}$ values are comparable to those in the title compound; however, the Δ_{br} values are approximately half of the value found here, *i.e.* the bond-length distortion (Renner & Lehmann, 1986) is smaller for the title compound (Table 1). The Ge3 tetrahedron [equivalent to *T*4 in Barbier (1995)] is much more regular and does not display a short Ge—O bond pointing towards the *M*-site layer as found in the title compound. However, the trioctahedral unit of Mn6–Mn6^{i}–Mn5 sites, to which atom O8 is bonded besides Ge3^{ii} [symmetry codes: (i) $-x+1, -y+2, -z$; (ii) $x, y, z-1$], exhibits a less uniform charge distribution in $Na_2(Mn_{5.26}Na_{0.74})Ge_6O_{20}$ than in the Barbier (1995) sample $Na_2(Mg_{3.6}Fe_{2.4})[(Ge_{5.6}Fe_{0.4})O_{18}]O_2$. Here *M*6 is exclusively occupied by Mg^{2+} and *M*5 has an $Mg_{0.74}{}^{2+}Fe_{0.26}{}^{3+}$ composition, while the title compound has – on the basis of bond-valence calculations (Brese & O'Keeffe, 1991) – an $Na_{0.74}{}^{+}Mn_{0.26}{}^{2+}$ and $Mn_{0.32}{}^{2+}Mn_{0.68}{}^{3+}$ composition for *M*6 and *M*5, respectively.

Generally, the GeO_4 tetrahedra are remarkably regular in the title compound. Both the tetrahedral angle variance (TAV) and the tetrahedral quadratic elongation (TQE) parameters (Robinson *et al.*, 1971) are low, the Ge5 and Ge6 tetrahedra being somewhat more regular than those within the tetrahedral chain. For comparison, distortion parameters found in other germanates are most frequently found in the ranges between 40 and 100° for TAV, and 1.01 and 1.02 for TQE (Redhammer & Roth, 2004*a*, 2006; Redhammer *et al.*, 2005, 2006, 2007*a*,*b*,*c*; Redhammer, Merz *et al.*, 2007). The most regular GeO_4 tetrahedra found so far are realized in $Cu_2Fe_2Ge_4O_{13}$ (the Ge3 site with TAV and TQE values of 1.6° and 1.0005; Redhammer, Merz *et al.*, 2007) and in $Cu(Cu_{0.44}Cr_{4.58})Ge_2O_{12}$ (with TAV and TQE values of 5.32° and 1.0013, respectively; Redhammer *et al.*, 2007*a*). The bond-valence sums of the Ge sites in the title compound are close to the expected value, the GeO_4 tetrahedra within the chain being slightly overbonded, while the 'attached' tetrahedra are somewhat underbonded.

The chain of Ge1–Ge4 tetrahedra is distinctly kinked in $Na_2(Mn_{5.26}Na_{0.74})Ge_6O_{20}$; the average O—O—O tetrahedral bridging angle is 146.4 (1)°, with the individual values ranging between 140.9 (1) and 152.1 (1)° (Table 1). A similar average kinking angle of 143.3° was found by Barbier (1995) for the Na–Mg–Fe germanate. These O—O—O angles compare well with the tetrahedral bridging angle in germanate clinopyroxenes, *e.g.* in synthetic $LiFeGe_2O_6$ [137.6 (1) and 151.1 (1)° for the *A* and *B* chain in the $P2_1/c$ phase at 298 K; Redhammer *et al.*, 2008] or in $CaCuGe_2O_6$ [with the *A* and *B* chains kinked by 139.3 (1) and 179.9 (1)° in the $P2_1/c$ phase at ~720 K, while the bridging angle is 159.4 (1)° in the $C2/c$ phase at ~800 K (Redhammer *et al.*, 2005)]. The aenigmatite-type silicate minerals show bridging angles that are larger by ~10–12°. The average *T*—O bond lengths in aenigmatite-type compounds are positively correlated with the average tetrahedral radius of the individual *T* sites (Table 1); however, no systematic variation is found for any polyhedral distortion parameter. This indicates that the distortional geometry of the tetrahedra is dominated by the geometry of the neighboring polyhedra, especially by the *M*-site cations and by the way in which O atoms are shared between neighbouring sites.

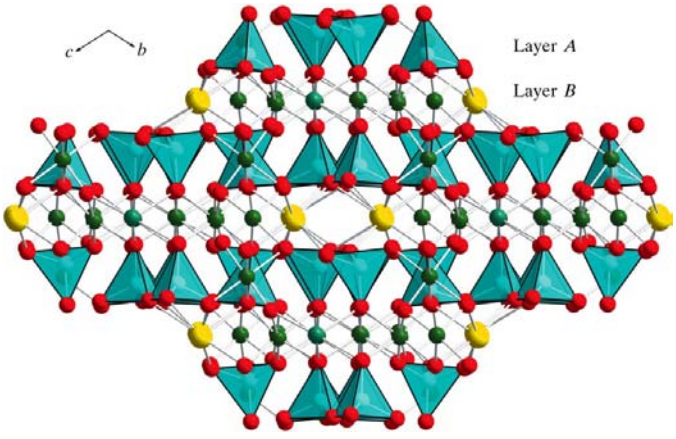

Figure 2
A polyhedral representation of the aenigmatite-type structure, viewed down the [100] direction, displaying the structure of stacked *A* and *B* layers.

The *M*1 and *M*2 octahedra connect individual chains of GeO_4 tetrahedra with each other along the *c* direction. Thereby, the apices of the tetrahedra alternate 'up' and 'down' (Figs. 2 and 3*a*). The isolated *M*1 and *M*2 sites are characterized by a small ⟨*M*—O⟩ bond length and are preferentially filled by trivalent or highly charged cations in the aenigmatite-type compounds. In krinovite, $Na_2Mg_4Cr_2Si_6O_{20}$, these two sites exclusively host Cr^{3+} (Bonaccorsi *et al.*, 1989), while in rhönite, $Ca_2(Mg, Fe, Ti)_6Si_6O_{20}$, *M*1 and *M*2 are characterized by high amounts of Ti^{4+} (Bonaccorsi *et al.*, 1990). On the basis of bond-valence considerations, Burt *et al.* (2007) state that *M*1 and *M*2 are filled by 84 and 70% Fe^{3+} in wilkinsonite, $Na_2Fe_6Si_6O_{20}$. Finally, Fe^{3+} clearly dominates Mg^{2+} in $Na_2(MgFe)[(GeFe)O_{18}]O_2$, having an occupation of 80% in *M*1 and *M*2. In most of the aenigmatite-type compounds, the average ⟨*M*1—O⟩ and ⟨*M*2—O⟩ distances are – together with ⟨*M*7—O⟩ – the smallest of all ⟨*M*—O⟩ bond lengths. This is also true for the title compound. On the basis of bond-valence calculations, the small ⟨*M*1—O⟩ and ⟨*M*2—O⟩ values of 2.037 (6) and 2.047 (5) Å indicate that Mn is almost exclusively in the trivalent state on these two sites. The *M*1 and *M*2 polyhedra connect the tetrahedral '*A*' layer with two neighboring '*B*' layers, by sharing four of their edges with the *M*5 and *M*7 octahedra (two edges each for the layer above and below the '*A*' layer). In comparison to other aenigmatite-type compounds, it is evident that Mn^{3+} with its $3d^4$ electronic configuration causes a distinct distortion to the *M*1 and *M*2 sites, expressed by a large BLD value but also by large octahedral angle variance and quadratic octahedral elongation parameters (Table 1). In the silicate aenigmatite-type minerals, these two polyhedra appear to be much more regular (Table 1); the Na–Mg–Fe germanate of Barbier (1995) also exhibits less polyhedral distortion.

The slab of *M* sites, which is the main building unit of the '*B*' layer in the aenigmatite structure (Figs. 2 and 3*b*), hosts the *M*3–*M*7 octahedra. The average *M*—O bond lengths range between 2.054 (5) and 2.321 (5) Å, reflecting the mixed occupation with Mn^{2+}, Mn^{3+} and Na^+. All three cations rarely occupy the *M* sites in aenigmatite-type compounds known so far. Thus, the *M*—O bond lengths in the title compound are amongst the largest reported. Using bond-valence analysis (Brese & O'Keeffe, 1991), Mn^{2+}/Mn^{3+} ratios on the different *M* sites have been determined in a manner similar to that described by Burt *et al.* (2007), giving Mn^{3+} percentages of, respectively, 38% on *M*3, 0% on *M*4, 32% on *M*5, 0% on *M*6 and 79% on *M*7; *M*1 and *M*2 are occupied by 100% Mn^{3+}, while for *M*6 the site occupancy is given as $Na_{0.74}Mn_{0.26}{}^{2+}$. Using these Mn^{2+}/Mn^{3+} ratios to calculate average cationic radii ⟨r_M⟩, a well defined positive correlation is valid between ⟨*M*—O⟩ and ⟨r_M⟩. This trend is well met by data from several other aenigmatite-type compounds (Fig. 4). All '*B*'-layer octahedra are connected to each other by corner sharing.

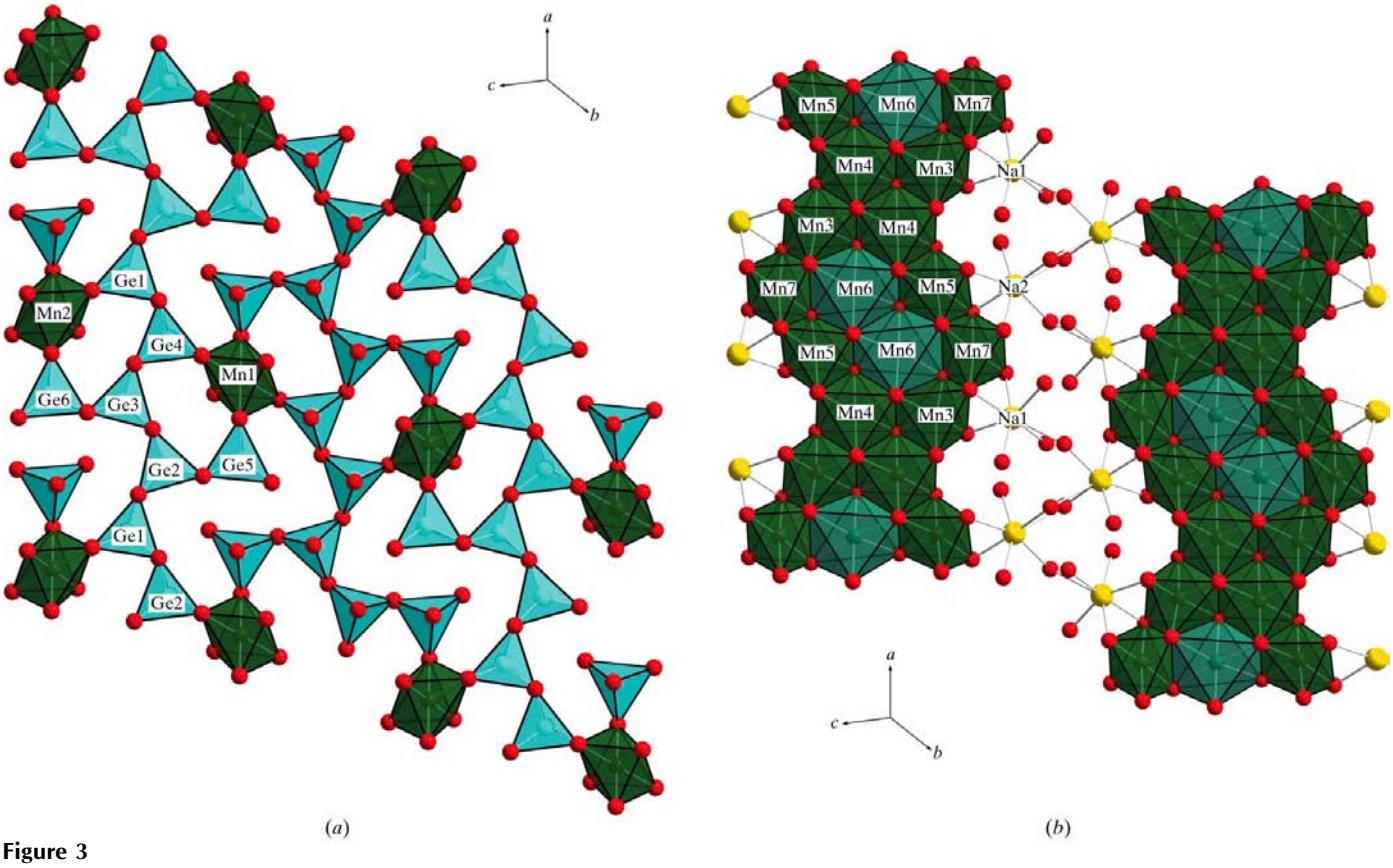

Figure 3
A polyhedral representation of the aenigmatite-type structure, viewed down the [111] direction, depicting (*a*) the Ge1–Ge6 '*A*' layer and (*b*) the slabs of the *M*-site '*B*' layers.

Along the *a* direction, a four-octahedron unit, consisting of two *M*3 and two *M*4 octahedra, alternates with a six-octahedron unit of two *M*5, two *M*6 and two *M*7 octahedra. The *M*6 polyhedron thereby is the only one that shares six of its edges with neighboring *M* polyhedra and shows – by far – the largest average *M*—O bond length. This is due to the presence of Na^+ at *M*6, a feature not reported so far for the aenigmatite structure type, but also due to the intense edge sharing with the neighboring sites. Among all *M* sites, the *M*6 octahedron is the most distorted; the value found for the title compound thereby is the largest reported so far for aenigmatite-type compounds. Generally, the *M*6 site deviates most from ideal octahedral geometry in the aenigmatite structure (Table 1). A rough positive correlation can be found between average cationic radius $\langle r_M \rangle$ and polyhedral distortion parameters, *e.g.* between $\langle r_M \rangle$ and OAV for some *M* sites; this is most evident for the *M*3 and *M*5 sites, while the polyhedral distortion of the *M*1, *M*2 and *M*7 octahedra appears to be independent of $\langle r_M \rangle$ and is dominated by geometric constraints from their neighboring sites. The *M*4 site displays the second largest $\langle M—O \rangle$ bond length, reflecting the fact – corroborated by the bond-valence sum – that this site is occupied by Mn^{2+} exclusively. It is this site which is the most regular in terms of bond length and angular distortion (Table 1). This can be regarded as additional evidence that *M*4 is occupied only by Mn^{2+} with its closed-shell $3d^5$ electronic configuration. In most aenigmatite-type compounds, except rhönite, the *M*4 site is occupied by divalent cations only. In contrast, the *M*7 site, sharing a common edge with the *M*1 site of the 'A' layer, preferentially accommodates highly charged cations, *e.g.* Fe^{3+} only in synthetic $Na_2(Mg,Fe)_6(Ge,Fe)_6O_{18}O_2$ (Barbier 1995), or Cr^{3+} in krinovite. From this charge distribution, it is evident that, within the '*B*'-layer *M*3–*M*7 octahedral slab, a central pyroxene-like zigzag chain of edge-sharing *M*4–*M*4–*M*6–*M*6–*M*4$\cdots$ octahedra can be identified which preferentially contains divalent cations or, more generally, cations with low charge, while the *M*3, *M*5 and *M*7 octahedra, attached to this chain, host – additionally or exclusively – trivalent or higher valent cations. This zigzag chain, which is closely related to the *M*1 chain of the clinopyroxene structure, reveals the very same interconnection with the chain of Ge1–Ge4 tetrahedra as is realized in the clinopyroxenes (Fig. 3*b*). Thus, an alternative description of the aenigmatite-type structure addresses pyroxene-like slabs, which alternate with spinel-like slabs (Barbier, 1995; Yang & Konzett, 2000).

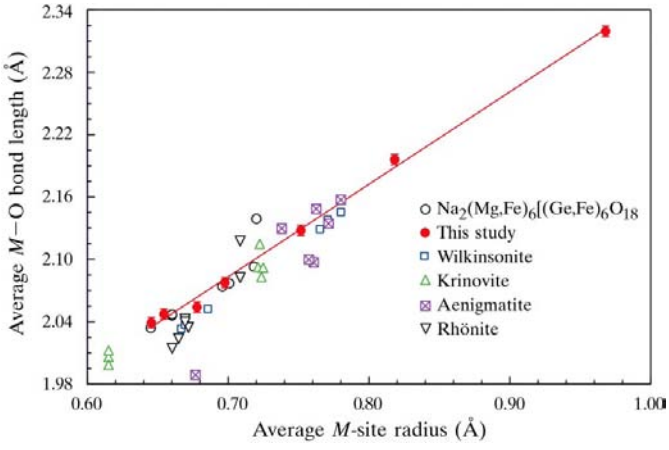

Figure 4
The correlation between average ionic radius $\langle r_M \rangle$ and $\langle M—O \rangle$ for the different *M* sites in different aenigmatite-type compounds.

A major difference between the title compound and other aenigmatite-type compounds lies in the coordination geometry of the Na^+ (*A*) cation. In the title compound, Na exhibits a (6+1)-fold coordination for both *A* sites, with six Na—O bonds between 2.346 (6) and 2.553 (6) Å, the seventh being 2.805 (6) and 2.793 (6) Å apart. The next nearest O atoms to Na1 and Na2 are 3.249 (6) and 3.234 (6) Å away and are regarded as nonbonding. A similar observation was made by Barbier (1995) for the synthetic NaMg germanate. These longest coordinating *A*—O bond lengths are distinctly shorter in the germanate compounds than in the silicate aenigmatites of Table 1, where the longest *A*—O bonds range between 2.95 and 3.06 Å. Barbier (1995) states that this (6+1)-fold coordination of the Na sites is intermediate between the (7+1)-fold coordination as found in, for example, aenigmatite (Cannillo *et al.*, 1971) and the sapphirine structure with the corresponding sixfold-coordinated Mg-rich sites (Barbier, 1995). The coordination of the *A*-site cations is directly related to the conformation state of the pyroxene-like tetrahedral chains. Silicate aenigmatite minerals with their (7+1)-coordination have average tetrahedal kinking angles above 150°, in the synthetic germanates the average kinking angles are 143.3 and 146.3°, while sappirine with the sixfold-coordinated Mg sites shows small tetrahedral kinking angles of 130.3° only. A well defined negative correlation is valid between the conformation state of the tetrahedral chain and the long distant *A*—O bonds, *i.e.* the more the tetrahedral chains are stretched, the closer the long distant O atoms are moved towards the *A* cations; in aenigmatite and wilkinsonite with the largest $\langle O—O—O \rangle$ angles, the eighth O atoms in the coordination polyhedron are ∼2.95 Å apart and have to be regarded as bonding O atoms leading to the (7+1)-fold coordination (Table 1). In the clinopyroxenes, the principal mechanism is similar but reversed: as the tetrahedral chain becomes stretched, the respective O atom corresponding to the largest distance moves out of the coordination environment of the *M*2 sites, most instructively displayed by the low-temperature behaviour upon the $C2/c$–$P2_1/c$ phase transitions in Li clinopyroxenes (Redhammer *et al.*, 2002, 2004*b*).

Experimental

As part of our crystal chemical investigations of (Na,Li)MGe$_2$O$_6$ 1:3 germanate clinopyroxene compounds (Redhammer *et al.*, 2008), the title compound was obtained accidentally during attempts to synthesize $NaMnGe_2O_6$ using flux growth methods. A finely ground and homogenized mixture of Na_2CO_3, Mn_2O_3 and GeO_2 in the stoichiometry $NaMnGe_2O_6$ was added to the high-temperature solvent (80 wt% Li_2MoO_4 and 20 wt% $LiVO_3$) in a ratio of educt to flux of 1 g:10 g. This starting material was placed in a platinum crucible, covered with a lid and heated in a chamber furnace to 1473 K, held for 24 h at this temperature, and cooled to 973 K at a

Table 1
Selected structural and distortional parameters for aenigmatite-type compounds.

Literature data recalculated from fractional atomic coordinates and lattice parameters given in the Inorganic Crystal Structure Database (ICSD, 2005).

	NMnG	NMgG	Wilkins	Mg-Aenig	Aenig	Rhönite	Krinovite
a (Å)	10.5578	10.495	10.3355	10.2925	10.4060	10.367	10.238
b (Å)	11.1532	10.876	10.7847	10.7052	10.8130	10.756	10.642
c (Å)	9.1833	8.994	8.9142	8..8027	8.9260	8.895	8.770
α (°)	106.707	105.9	105.048	105.280	104.930	105.98	105.15
β (°)	95.809	95.9	96.461	96.712	96.870	96.04	96.50
γ (°)	124.367	124.7	125.302	125.256	125.320	124.72	125.15
⟨*M*1—O⟩ (Å)	2.037	2.046	2.033	2.0378	2.097	2.0238	2.0062
⟨O—O⟩ (Å)	2.880	2.891	2.874	2.8805	2.963	2.860	2.8347
V (Å^3)	10.986	11.264	11.113	11.213	12.088	10.939	10.640
BLD[a] (%)	5.06	0.85	1.16	0.90	3.06	0.36	1.28
OAV[b] (°)	47.67	31.11	18.98	14.67	37.46	23.17	26.43
OQE[c]	1.0207	1.0094	1.0060	1.0043	1.0122	1.0069	1.0080
S[d] (v.u.)	2.97	2.58	2.87	2.37	2.27	2.46	2.80
⟨*M*2—O⟩ (Å)	2.047	2.047	2.052	2.0638	2.100	2.014	2.0124
⟨O—O⟩ (Å)	2.894	2.892	2.901	2.9171	2.967	2.847	2.8432
V (Å^3)	11.154	11.265	11.400	11.606	12.099	10.804	10.7224
BLD[a] (%)	5.19	0.97	2.78	1.99	3.17	0.26	1.52
OAV[b] (°)	46.374	33.802	22.911	21.557	43.439	20.029	30.002
OQE[c]	1.0207	1.0104	1.0083	1.0072	1.0148	1.0059	1.0092
S[d] (v.u.)	2.90	2.58	2.75	2.22	2.09	2.51	2.81
⟨*M*3—O⟩ (Å)	2.128	2.074	2.138	2.100	2.134	2.083	2.093
⟨O—O⟩ (Å)	3.004	2.927	3.014	2.967	3.006	2.941	2.956
V (Å^3)	12.492	11.666	12.663	12.214	12.530	11.828	12.090
BLD[a] (%)	2.66	1.83	3.25	1.40	3.17	0.79	1.24
OAV[b] (°)	60.146	42.721	63.429	26.595	75.414	40.210	25.339
OQE[c]	1.0198	1.0135	1.0209	1.0080	1.0245	1.0121	1.0073
S[d] (v.u.)	2.45	2.41	2.06	2.01	2.09	2.09	2.04
⟨*M*4—O⟩ (Å)	2.196	2.093	2.145	2.101	2.157	2.043	2.092
⟨O—O⟩ (Å)	3.101	2.955	3.029	2.959	3.047	2.883	2.951
V (Å^3)	13.872	12.046	12.994	12.065	13.204	11.179	11.931
BLD[a] (%)	1.10	0.90	1.68	2.18	1.43	1.70	2.04
OAV[b] (°)	42.761	33.105	30.898	56.436	31.942	35.492	51.919
OQE[c]	1.0123	1.0100	1.0093	1.0171	1.0095	1.0113	1.0162
S[d] (v.u.)	2.01	2.04	1.99	2.01	1.92	2.35	2.06
⟨*M*5—O⟩ (Å)	2.076	2.077	2.129	2.082	2.130	2.035	2.083
⟨O—O⟩ (Å)	2.932	2.930	2.999	2.930	2.998	2.872	2.935
V (Å^3)	11.677	11.712	12.556	11.752	12.511	11.073	11.772
BLD[a] (%)	3.67	1.69	2.62	2.07	2.37	1.50	1.92
OAV[b] (°)	42.737	44.839	53.818	54.837	64.533	30.984	51.957
OQE[c]	1.0162	1.0140	1.0174	1.0168	1.0203	1.0098	1.0163
S[d] (v.u.)	2.61	2.39	2.09	2.12	2.09	2.40	2.11
⟨*M*6—O⟩ (Å)	2.321	2.139	2.156	2.100	2.1485	2.118	2.115
⟨O—O⟩ (Å)	3.270	3.015	3.043	2.965	3.032	2.988	2.984
V (Å^3)	15.596	12.512	12.952	12.037	12.704	12.186	12.221
BLD[a] (%)	3.28	1.63	1.09	1.20	1.10	1.81	0.67
OAV[b] (°)	141.758	89.629	73.904	56.889	88.392	81.613	72.076
OQE[c]	1.0466	1.0282	1.0217	1.0175	1.0273	1.026	1.0215
S[d] (v.u.)	1.47	1.91	1.92	2.00	1.96	1.92	1.92
⟨*M*7—O⟩ (Å)	2.054	2.034	2.037	2.037	1.989	2.040	1.999
⟨O—O⟩ (Å)	2.903	2.876	2.881	2.874	2.8151	2.885	2.827
V (Å^3)	11.324	11.084	11.133	11.110	10.410	11.167	10.520
BLD[a] (%)	2.21	2.72	2.01	1.06	4.47	3.59	2.82
OAV[b] (°)	44.610	27.425	28.537	34.456	17.918	30.844	26.539
OQE[c]	1.0140	1.0086	1.0087	1.0100	1.0078	1.0103	1.0088
S[d] (v.u.)	2.74	2.71	2.85	2.37	3.14	2.41	2.90
⟨*T*1—O⟩ (Å)	1.747	1.766	1.637	1.621	1.651	1.7098	1.624
⟨O—O⟩ (Å)	2.847	2.876	2.669	2.644	2.692	2.787	2.650
V (Å^3)	2.709	2.791	2.232	2.173	2.288	2.541	2.190
BLD[a] (%)	1.37	0.63	1.25	1.44	0.83	0.42	1.06
TAV[e] (°)	29.016	34.262	24.719	15.810	28.163	27.054	12.434
TQE[f]	1.0070	1.0083	1.0059	1.0037	1.0067	1.0064	1.0029
S[d] (v.u.)	4.03	3.82	–	4.05	3.71	3.17	–
⟨*T*2—O⟩ (Å)	1.742	1.750	1.632	1.631	1.654	1.724	1.616
⟨O—O⟩ (Å)	2.838	2.853	2.663	2.663	2.700	2.810	2.637
V (Å^3)	2.686	2.728	2.222	2.221	2.316	2.592	2.154
BLD[a] (%)	0.94	0.63	0.98	0.97	0.38	0.33	1.11
TAV[e] (°)	26.995	22.806	12.498	8.830	10.024	36.369	14.913
TQE[f]	1.0061	1.0053	1.0029	1.0022	1.0024	1.0097	1.0036
S[d] (v.u.)	4.07	3.98	–	3.92	3.68	3.05	
⟨*T*3—O⟩ (Å)	1.733	1.735	1.621	1.625	1.627	1.675	1.628
⟨O—O⟩ (Å)	2.826	2.829	2.645	2.649	2.656	2.731	2.654
V (Å^3)	2.656	2.662	2.178	2.178	2.206	2.393	2.189
BLD[a] (%)	1.08	0.46	0.91	1.10	0.59	0.74	0.90
TAV[e] (°)	15.626	17.665	10.762	30.339	8.080	20.270	33.702
TQE[f]	1.0035	1.0041	1.0026	1.0071	1.0019	1.0048	1.0079
S[d] (v.u.)	4.15	4.15	–	4.00	3.97	3.49	
⟨*T*4—O⟩ (Å)	1.741	1.750	1.631	1.646	1.627	1.692	1.640
⟨O—O⟩ (Å)	2.839	2.851	2.659	2.683	2.653	2.758	2.673
V (Å^3)	2.692	2.719	2.206	2.266	2.193	2.458	2.238
BLD[a] (%)	0.97	0.45	0.89	1.44	1.19	0.23	0.69
TAV[e] (°)	17.464	34.442	24.390	29.323	21.411	30.192	29.194
TQE[f]	1.0041	1.0082	1.0057	1.0071	1.0051	1.0077	1.0072
S[d] (v.u.)	4.07	3.97	–	3.78	3.97	3.28	
⟨*T*5—O⟩ (Å)	1.756	1.759	1.637	1.643	1.640	1.737	1.639
⟨O—O⟩ (Å)	2.865	2.868	2.670	2.679	2.676	2.834	2.674
V (Å^3)	2.766	2.777	2.237	2.258	2.254	2.671	2.249
BLD[a] (%)	1.62	0.72	1.07	1.56	1.07	1.45	1.43
TAV[e] (°)	14.993	16.137	14.724	20.072	9.630	17.682	14.319
TQE[f]	1.0038	1.0040	1.0037	1.0052	1.0025	1.0052	1.0036
S[d] (v.u.)	3.92	3.88	–	3.82	3.84	2.92	
⟨*T*6—O⟩ (Å)	1.762	1.760	1.635	1.643	1.632	1.743	1.640
⟨O—O⟩ (Å)	2.874	2.868	2.667	2.679	2.662	2.842	2.674
V (Å^3)	2.792	2.774	2.231	2.259	2.219	2.692	2.248
BLD[a] (%)	1.30	0.81	1.02	1.09	1.16	1.69	1.13
TAV[e] (°)	14.124	22.937	14.220	22.519	12.520	20.322	18.229
TQE[f]	1.0036	1.0058	1.0035	1.0057	1.0030	1.0062	1.0045
S[d] (v.u.)	3.87	3.87	–	3.80	3.92	2.88	
O4—O3—O6	149.69	145.94	160.50	160.26	160.75	155.48	162.18
O3—O6—O10	152.05	148.16	163.89	150.98	163.15	149.56	152.99
O6—O10—O4	142.84	141.04	154.11	148.90	154.10	146.52	149.50
O10—O4—O3	140.92	138.53	150.80	157.98	151.81	152.20	158.61
⟨O—O—O⟩	146.38	143.32	157.33	154.528	157.45	150.94	155.82
CN *A*1[g]	6+1	6+1	7+1	7+1	7+1	7+1	7+1
⟨*A*1—O⟩	2.494	2.447	2.544	2.525	2.548	2.516	2.512
*A*1—O$_{long}$[h]	2.805	2.856	2.965	3.011	2.948	3.016	2.965
⟨*A*1—O⟩$_{6.7}$	2.440	2.397	2.484	2.456	2.490	2.435	2.447
S[d] (v.u.)	1.15	1.28	–	1.22	1.11	2.04	1.25
CN *A*2[g]	6+1	6+1	7+1	7+1	7+1	7+1	7+1
⟨*A*2—O⟩	2.499	2.463	2.557	2.544	2.570	2.529	2.524
*A*2—O$_{long}$[h]	2.793	2.830	2.983	3.015	2.969	3.056	2.953
⟨*A*2—O⟩$_{inner}$	2.450	2.402	2.496	2.477	2.513	2.444	2.463
S[d] (v.u.)	1.14	1.20	–	1.19	1.07	1.98	1.21

Notes: NMnG = title compound, this study; NMgG = $Na_2(Mg_{3.6}Fe_{2.4})[(Ge_{5.6}Fe_{0.4})O_{18}]O_{20}$ (Barbier, 1995); Wilkins = wilkinsonite, $Na_2Fe_4^{2+}Fe_2^{3+}Si_6O_{20}$ (Burt *et al.*, 2007); Mg-Aenig = Mg-aenigmatite, $Na_2Mg_6Si_6O_{18}(OH)_2$ (Yang & Konzett, 2000); Aenig = aenigmatite, $Na_2Fe_5TiSi_6O_{20}$ (Cannillo *et al.*, 1971); Rhönite = $Ca_2(Mg,Fe,Ti)_6Si_6O_{20}$ (Bonaccorsi *et al.*, 1990); Krinovite = $Na_2Mg_4Cr_2Si_6O_{20}$ (Bonaccorsi *et al.*, 1989). (*a*) Bond length distortion, BLD = $(100/n)\sum_{i=1}^{n}\{[(X—O)_i - \langle x—O\rangle]/\langle X—O\rangle\}$, with n = number of bonds, $(X—O)_i$ = central cation-to-oxygen length and ⟨X—O⟩ = average cation–oxygen bond length (Renner & Lehmann, 1986). (*b*) Octahedral angle variance, OAV = $\sum_{i=1}^{n}(\Theta_i - 90)^2/11$ (Robinson *et al.*, 1971). (*c*) Octahedral quadratic elongation, OQE = $\sum_{i=1}^{6}(l_i/l_o)^2/6$, with l_o = centre-to-vertex distance for a regular octahedron whose volume is equal to that of the undistorted octahedron with bond length l_i (Robinson *et al.*, 1971). (*d*) Bond-valence sum, S (Brese & O'Keeffe, 1991). (*e*) Tetrahedral angle variance, TAV = $\sum_{i=1}^{n}(\Theta_i - 109.47)^2/5$ (Robinson *et al.*, 1971). (*f*) Tetrahedral quadratic elongation, TQE = $\sum_{i=1}^{4}(l_i/l_t)^2/4$, with l_t = centre-to-vertex distance for a regular tetrahedron whose volume is equal to that of the undistorted tetrahedron with bond length l_i (Robinson *et al.*, 1971). (*g*) CN = number of *A*1 (Na, Ca) coordinating O atoms. (*h*) Denotes the longest A—O bond length.

rate of 1.8 K h^{-1}. After dissolution of the flux in hot distilled water, dark-brown-to-black needle-like crystals were obtained. Chemical analysis was performed on three different grains using an electron microprobe, indicating 7.60% Na_2O, 33.62% MnO and 56.42 GeO_2 by weight; no other elements are present in the sample, as proved by energy dispersive X-ray analysis. On the basis of 20 O atoms and the Mn^{2+}/Mn^{3+} ratio extracted from bond-valence calculations, this gives rise to the structural formula $Na_{2.73\ (2)}Mn_{5.28\ (1)}Ge_{6.01\ (2)}O_{20}$, which is identical to the formula derived from structure refinement within experimental error.

Crystal data

$Na_2(Mn_{5.26}Na_{0.74})Ge_6O_{20}$	γ = 124.367 (5)°
M_r = 1107.49	V = 806.05 (11) Å^3
Triclinic, $P\overline{1}$	Z = 2
a = 10.5578 (9) Å	Mo $K\alpha$ radiation
b = 11.1532 (7) Å	μ = 15.17 mm^{-1}
c = 9.1833 (7) Å	T = 295 (2) K
α = 106.707 (2)°	0.09 × 0.07 × 0.04 mm
β = 95.809 (1)°	

Data collection

Bruker SMART APEX diffractometer	9401 measured reflections
	3400 independent reflections
Absorption correction: numerical *via* equivalents using *X-SHAPE* (Stoe & Cie, 1996)	2545 reflections with $I > 2\sigma(I)$
	R_{int} = 0.073
T_{min} = 0.29, T_{max} = 0.55	

Refinement

$R[F^2 > 2\sigma(F^2)]$ = 0.042	313 parameters
$wR(F^2)$ = 0.082	1 restraint
S = 0.95	$\Delta\rho_{max}$ = 1.22 e Å^{-3}
3400 reflections	$\Delta\rho_{min}$ = −1.03 e Å^{-3}

Structure solution using Patterson methods (Sheldrick, 1997) yielded the Ge and Mn positions; O atoms and Na atoms were localized from difference Fourier map analysis. After full anisotropic refinement against F^2 with all the M sites filled with Mn, it became evident that the Mn6 site is partly empty or partly substituted. Allowing the site-occupation factor of Mn6 to refine freely yielded an occupation of 0.43 Mn, significantly below the expected value of 1, and a drop of the $R1$ value by nearly 4%. As chemical analysis showed an Na content above the expected 2.0 formula units, a mixed occupation of $M6$ with Mn and Na was tested. The refinement converged to an occupation very close to that expected from chemical analysis.

Data collection: *SMART-Plus* (Bruker, 2001); cell refinement: *SAINT-Plus* (Bruker, 2001); data reduction: *SAINT-Plus*; program(s) used to solve structure: *SHELXS97* (Sheldrick, 2008); program(s) used to refine structure: *SHELXL97* (Sheldrick, 2008); molecular graphics: *DIAMOND* (Version 3.0; Brandenburg & Berndt, 1999); software used to prepare material for publication: *WinGX* (Version 1.70.01; Farrugia, 1999).

GJR gratefully acknowledges financial support by the 'Fonds zur Förderung der wissenschaftlichen Forschung (FWF)', Vienna, Austria, under grants R33-N10 (Erwin-Schrödinger Rückkehr-Stipendium) and P19762-N10.

Supplementary data for this paper are available from the IUCr electronic archives (Reference: IZ3033). Services for accessing these data are described at the back of the journal.

References

Barbier, J. (1995). *Z. Kristallogr.* **210**, 19–23.
Barbier, J., Grew, E. S., Halenius, E., Halenius, U. & Yates, G. (2002). *Am. Mineral.* **87**, 501–513.
Bonaccorsi, E., Merlino, S. & Pasero, M. (1989). *Z. Kristallogr.* **187**, 133–138.
Bonaccorsi, E., Merlino, S. & Pasero, M. (1990). *Eur. J. Mineral.* **2**, 203–218.
Brandenburg, K. & Berndt, M. (1999). *DIAMOND*. Crystal Impact GbR, Bonn, Germany.
Brese, N. E. & O'Keeffe, M. (1991). *Acta Cryst.* B**47**, 192–197.
Bruker (2001). *SMART-Plus* (Version 5.6) and *SAINT-Plus* (Version 5.0). Bruker AXS Inc., Madison, Wisconsin, USA.
Burt, J. B., Downs, R. T. & Costin, G. (2007). *Acta Cryst.* E**63**, i122–i124.
Cannillo, E., Mazzi, F., Fang, J. H., Robinson, P. D. & Ohya, Y. (1971). *Am. Mineral.* **56**, 427–446.
Farrugia, L. J. (1999). *J. Appl. Cryst.* **32**, 837–838.
Gasparik, T., Parise, J. B., Young, V. G. Jr & Wilford, W. S. (1999). *Am. Mineral.* **84**, 257–266.
Grew, E. S., Barbier, J., Britten, J., Hålenius, U. & Shearer, C. K. (2007). *Am. Mineral.* **92**, 80–90.
Grew, E. S., Barbier, J., Britten, J., Yates, M. G., Polyakov, V. O., Shcherbakova, E. P., Halenius, U. & Shearer, C. K. (2005). *Am. Mineral.* **90**, 1402–1412.
ICSD (2005). Inorganic Crystal Structure Database. FIZ-Karlsruhe, Germany, and the National Institute of Standards and Technology (NIST), USA.
Kunzmann, Th. (1999). *Eur. J. Mineral.* **11**, 743–756.
Merlino, S. (1972). *Z. Kristallogr.* **136**, 81–88.
Merlino, S. (1980). *Z. Kristallogr.* **151**, 91–100.
Redhammer, G. J., Merz, M., Tippelt, G., Sparta, K., Roth, G., Treutmann, W., Lottermoser, W. & Amthauer, G. (2007). *Acta Cryst.* B**63**, 4–16.
Redhammer, G. J. & Roth, G. (2002). *Z. Kristallogr.* **217**, 63–72.
Redhammer, G. J. & Roth, G. (2004*a*). *J. Solid State Chem.* **177**, 2714–2725.
Redhammer, G. J. & Roth, G. (2004*b*). *Z. Kristallogr.* **219**, 278–294.
Redhammer, G. J. & Roth, G. (2006). *Acta Cryst.* C**62**, i61–i63.
Redhammer, G. J. & Roth, G. (2008). *Acta Cryst.* B**64**. In preparation.
Redhammer, G. J., Roth, G. & Amthauer, G. (2006). *Acta Cryst.* C**62**, i94–i96.
Redhammer, G. J., Roth, G. & Amthauer, G. (2007*a*). *Acta Cryst.* C**63**, i21–i24.
Redhammer, G. J., Roth, G. & Amthauer, G. (2007*b*). *Acta Cryst.* C**63**, i47–i50.
Redhammer, G. J., Roth, G. & Amthauer, G. (2007*c*). *Acta Cryst.* C**63**, i69–i72.
Redhammer, G. J., Tippelt, G., Merz, M., Roth, G., Treutmann, W. & Amthauer, G. (2005). *Acta Cryst.* B**61**, 367–380.
Renner, B. & Lehmann, G. (1986). *Z. Kristallogr.* **175**, 43–59.
Robinson, K., Gibbs, G. V. & Ribbe, P. H. (1971). *Science*, **172**, 567–570.
Sheldrick, G. M. (2008). *Acta Cryst.* A**64**, 112–122.
Stoe & Cie (1996). *X-SHAPE* and *X-RED*. Stoe & Cie, Darmstadt, Germany.
Yang, H. & Konzett, J. (2000). *Am. Mineral.* **85**, 259–262.